Available online at www.sciencedirect.com
ScienceDirect
Journal of Solid State Chemistry 179 (2006) 2965–2971
JOURNAL OF SOLID STATE CHEMISTRY
www.elsevier.com/locate/jssc

X-ray, Raman and FTIRS studies of the microstructural evolution of zirconia particles caused by the thermal treatment

Dmitry A. Zyuzin[a,*], Svetlana V. Cherepanova[a], Ella M. Moroz[a], Elena B. Burgina[a], Vladislav A. Sadykov[a], Victor G. Kostrovskii[b], Valerii A. Matyshak[c]

[a]*Boreskov Institute of Catalysis SB RAS, pr. Akademika Lavrentieva 5, 630090 Novosibirsk, Russia*
[b]*Institute of Solid State Chemistry SB RAS, 630090 Novosibirsk, Russia*
[c]*Semenov Institite of Chemical Physics RAS, Moscow, Russia*

Received 26 October 2005; received in revised form 26 February 2006; accepted 8 April 2006
Available online 22 May 2006

Abstract

Genesis of the structure of zirconia particles prepared by precipitation of amorphous hydrated zirconia by ammonia from the $ZrO(NO_3)_2$ solution followed by a mild hydrothermal treatment (HTT) of precipitate, washing and calcination under air up to 1000 °C has been studied by X-ray diffraction (XRD), Raman and FTIRS. As revealed by FTIRS of lattice modes, the local structure of amorphous zirconia subjected to HTT is close to that in m-ZrO_2. This helps to obtain nearly single-phase monoclinic nanozirconia (particle size 5–15 nm) already after a mild calcination at 500 °C. Stability of this phase with nanoparticles sizes below the critical value determined by thermodynamic constraints is due to its excessive hydroxylation demonstrated by FTIRS. Dehydroxilation and sintering of these nanoparticles at higher (600–650 °C) temperatures of calcination leads to reappearance of the (111) "cubic" reflection in XRD patterns. Modeling of XRD patterns revealed that this phenomenon could be explained by polysynthetic (001) twinning earlier observed by HRTEM.

Keywords: Monoclinic zirconia; Hydrothermal treatment; Polysynthetic twinning; Whole XRD pattern modeling

1. Introduction

Zirconia is one of the most refractory, shock-resistant and corrosion-resistant oxides, which determines its broad industrial application including construction ceramics, corrosion-resistant and thermal-barrier coatings, gas sensors, solid electrolytes, etc. [1,2]. Pure zirconia is also used as a dispersed phase in both oxide and non-oxide ceramics to increase fracture toughness, strength and hardness [3]. Dispersed zirconia attracts great attention as a catalyst or as a support for metal/oxide catalysts of red–ox/acid–base reactions [4–8].

As an attractive option for synthesis of dispersed zirconia, the hydrothermal treatment (HTT) at moderate (100–200 °C) temperatures of a hydrous zirconia precipitated by ammonia from inorganic salts (nitrates or chlorides) can be considered [9–11]. Any future practical application of such a technique requires elucidation of the features of zirconia phase composition and real/defect structure evolution in the course of subsequent progressive annealing under air at increasing temperatures. For the catalytic application, the phase composition and the real/defect structure of zirconia determine the surface density and strength of Lewis and Broensted acid sites [4–8,12] responsible for the reagents activation and/or anchoring of supported active components. However, the details of the real structure of these nanosized zirconia samples remain to be poorly characterized, and factors controlling them are not properly elucidated.

In a previous paper [13], evolution of the defect structure of nanosized zirconia particles prepared by HTT of precipitated amorphous zirconium hydroxide and calcined at temperatures in the range of 300–1000 °C was followed by using HRTEM. However, TEM is rather poorly sensitive to the local coordination environment of Zr

*Corresponding author. Fax: +7 383 3308056.
E-mail address: zyuzin@catalysis.nsk.su (D.A. Zyuzin).

0022-4596/$ - see front matter © 2006 Elsevier Inc. All rights reserved.
doi:10.1016/j.jssc.2006.04.057

cations, which can be changed due to generation of defects. In addition, TEM data by itself are not easily referred to the average structural features of dispersed samples, so there is a danger of overestimation of the occurrence of some structural features revealed by this method. Hence, the relative importance of different defects revealed by TEM for the average structural characteristics of samples is to be estimated by using X-ray (powder) diffraction (XRD). Similarly, spectroscopic methods (Raman, IR spectroscopy) are well known to be much more sensitive to the local distortion of coordination polyhedra in oxides as compared with XRD. Hence, the aim of the second paper of the series is to compare HRTEM data with the results of the same system studies by XRD, Raman and FTIRS of lattice modes.

2. Experimental

Samples of zirconia were prepared by a method similar to that described in [11]. As a starting compound, commercial product $ZrO(NO_3)_2$ of a high purity grade was used. Freshly prepared 1.5 M solution was aged for 15 h at room temperature. Hydrolysis of this solution was carried out at nearly constant pH value ~9.5 by rapidly adding it to the aqueous ammonia solution under intensive stirring. Thus obtained sol was subjected to HTT in the mother liquor in an autoclave first for 24 h at 90 °C and then at 110 °C for 8 h.

After cooling suspension and filtering precipitate, the latter was thoroughly washed by 0.1 M solution of NH_4OH and dried at 110 °C. Dried sample was separated into parts then calcined at 300, 400, 500, 560, 600, 650, 750 and 1000 °C under air in a muffle furnace. The temperature ramp includes heating from ~25 °C to required temperature, keeping at this temperature for 4 h followed by a slow cooling down in a muffle to room temperature after turning-off the power.

XRD patterns were obtained by using HZG-4C diffractometer by scanning in the 2Θ range 10–70° with a step of 0.05° and acquisition time in each point 10 s. Cu$K\alpha$ radiation monochromatized by passing through the graphite monochromator situated in a diffraction beam was used. Qualitative phase analysis has been carried out by using JCPDS–ICDD files and ICSD/retrieve database. Diffraction pattern treatment for the quantitative phase analysis has been carried out by using the PowderCell for Windows software and approximation of diffraction peaks by Pseudo-Voight function in the Origin® software. Estimation of the amount of monoclinic phase has also been carried out by using the expression:

$$\phi_{mon} = \frac{I^{mon}_{111} + I^{mon}_{\bar{1}11}}{I^{mon}_{111} + I^{mon}_{\bar{1}11} + I^{cub}_{111}},$$

where I^{i}_{111} is the integral intensity of the (111) peak of a given phase estimated by using area of the corresponding diffraction peak [14]. In addition, an amount of the monoclinic phase was determined by using the external standard method and the integral intensities of ($\bar{1}11$) and (111) diffraction peaks. Sample of ZrO_2 calcined at 1000 °C was chosen as such a standard. The X-ray particle sizes in the [111] and [202] directions for monoclinic phase and in the [111] direction for the cubic phase were estimated from the FWHM of corresponding diffraction peaks.

Modeling of diffraction patterns for nanoparticles of the monoclinic phase with a different real structure has been carried out by using approaches developed elsewhere [15].

Infra-red spectra of samples in the 200–4000 cm^{-1} range were registered using a BOMEM MB-102 spectrometer with resolution 4 cm^{-1}. Samples for measurements were prepared by a standard procedure of pressing wafers comprised of 3 mg of zirconia powder with 600 mg of CsI.

The Raman scattering measurements were carried out using a 100/S-Bruker Raman Fourier Spectrometer. The 1.06 mm line of an Nd–YAG laser was used for excitation, an output laser power was 100 mW.

3. Results and discussion

3.1. XRD

Fig. 1 shows fragments of the diffraction patterns of studied samples. Data on the qualitative phase analysis and X-ray particle sizes are presented in Table 1. Due to a high dispersion and superposition of peaks corresponding to different zirconia phases, it was impossible to clarify the space group of a highly symmetric phase, which will be tentatively termed henceforth as a "cubic" one.

As follows from the data presented in Fig. 1 and Table 1, there is a non-monotonous variation of the phase composition with the temperature of calcination. On one hand, as follows from the presence of the diffraction peak at $2\Theta = 30.25°$ and its intensity variation, the cubic phase first practically disappears at 500 °C reappearing again after annealing at 600 °C in an amount ~20%. On the

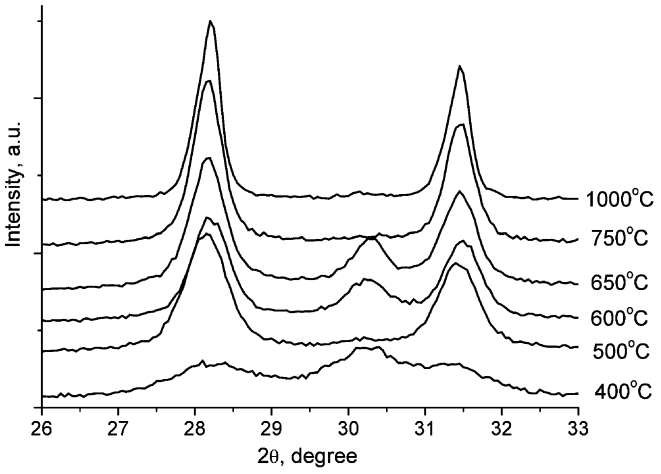

Fig. 1. Experimental diffraction patterns of zirconia samples calcined at different temperatures.

Table 1
X-ray data for samples of ZrO_2 calcined at different temperatures

Calcination temperature (°C)	Monoclinic ZrO_2			Cubic ZrO_2	
	Content (%)	D_{111} (Å)	D_{202} (Å)	Content (%)	D_{111} (Å)
400	44 (39)[a]	75	—	56	75
500	96 (92)	165	165	4	110
600	82 (97)	190	240	18	150
650	79 (99)	205	235	21	190
750	96 (97)	260	260	4	—
1000	96 (100)	400	400	4	—

[a]The amount of m-ZrO_2 determined by the external standard method is given in parenthesis.

other hand, as judged by the monoclinic phase peaks intensity, its amount is nearly constant under studied annealing conditions being close to 100% as estimated by using the external standard. This result agrees with the TEM data [13] revealing presence of only m-ZrO_2 particles in a sample annealed at 500 °C and appearance of fragments with a t-ZrO_2 structure as thin slabs between the twin boundaries in samples annealed at 650 °C.

For samples annealed at 400 and 500 °C, the X-ray particle sizes of both m- and c-phases are practically identical coinciding with those estimated by TEM [13]. This agrees with conclusions about the absence of extended defects in zirconia nanoparticle even after c–m martensitic transformation. For samples calcined at 600 and 650 °C, X-ray particle sizes of the monoclinic phase estimated for various directions were found to differ noticeably. Thus, the ($\bar{1}11$) and (111) diffraction peaks situated in the 2Θ range 28–32° are broader than the (202) peak situated at a higher diffraction angle ($2\Theta = 54.1°$). As a result, the particle sizes calculated for the [111] direction are smaller than those for the [202] direction. This suggests existence of additional defects due to a specific real/defect structure of those samples containing monoclinic phase, which can be polysynthetic twins revealed by HRTEM [13].

2. FTIRS and Raman spectroscopy

In the IR spectrum of the amorphous hydroxide dried at ~100 °C, practically the same spectral features as for samples calcined at higher temperatures and containing exclusively m-ZrO_2 are observed (Fig. 2). For the tetragonal zirconia phase, where Zr atom is surrounded by eight O atoms forming a distorted cube [17], only two bands at ~460 and ~670 cm^{-1} corresponding to IR-active E_u and A_{2u} modes should be observed [16]. Hence, at least for a part of Zr cations in the amorphous hydroxide subjected to HTT and dried, their local coordination is apparently strongly distorted resembling that in m-ZrO_2. In olygomerized band-like or sheet-like zirconium, polynuclear hydroxospecies based on the tetramer $[Zr_4(\mu\text{-}OH)_8(OH)_8(H_2O)_8]\times H_2O$ [18], Zr cations are also coordinated by eight hydroxyls and water molecules. Hence, HTT appears

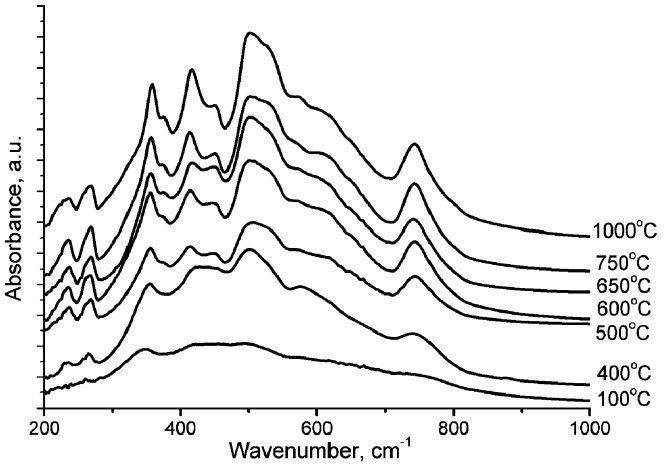

Fig. 2. The IR spectra of the lattice modes of zirconia samples calcined at different temperatures.

to facilitate polymerization of tetrameric species through their progressive dehydroxylation (oxolation) into less symmetric 3D structures with a local coordination of Zr resembling that in m-ZrO_2. Certainly, the presence of more symmetric species in amorphous hydroxide is not excluded as well, since broad IR bands do not allow to make more detailed analysis. At least, a high amount of water and hydroxyls in the amorphous hydroxide reflected in the high intensity of IR bands at ~3400 and ~1600 cm^{-1} (Fig. 3) corresponding to stretching and bending vibration modes of the water molecules [19] suggests that more symmetric structures with a local coordination similar to that in the tetrameric units are present as well.

After calcinations at 400 °C, the intensity of the water bands strongly declines (Fig. 3). In the lattice mode range (Fig. 2), IR bands at 232, 264, 354, 420–450, 501, 576 and 741 cm^{-1} are clearly resolved, which can be assigned to the monoclinic phase [20,21]. The Raman spectrum for this sample (Fig. 4) is of a low intensity. However, lines at 180, 188, 223, 234, 305, 333, 345, 378, 475, 505, 534, 569, 618 and 634 cm^{-1} typical for the m-ZrO_2 [20–25] can be identified. In addition, less intense lines at 140–150 and

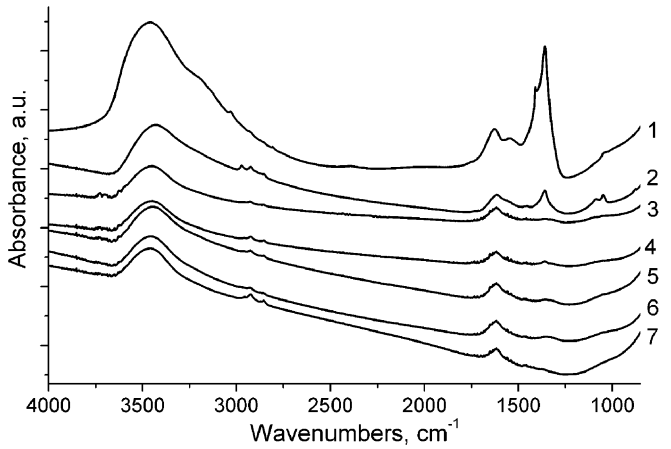

Fig. 3. The IR spectra in the H_2O range of zirconia samples calcined at different temperatures (°C).

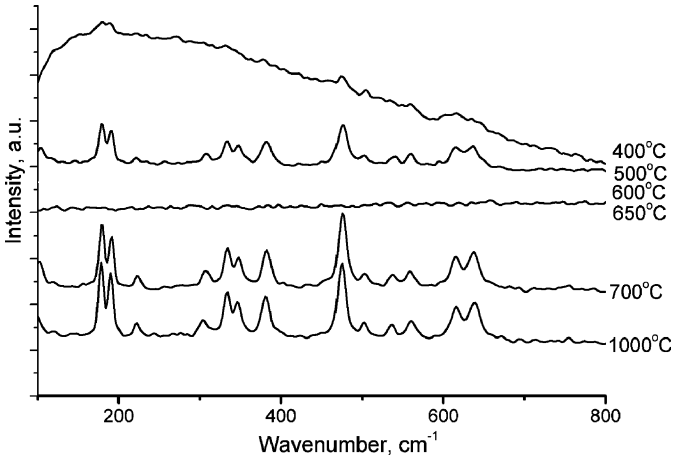

Fig. 4. The Raman spectra of zirconia samples calcined at different temperatures.

~270 cm^{-1} characteristic for the t-ZrO_2 phase [16,20–26] are observed. The most intense Raman line of the cubic phase at ~630 cm^{-1}, even if present, could not be apparently observed being superimposed with the more intense lines of the m-zirconia at ~618 and 634 cm^{-1}. Hence, this sample appears to be a mixture of the tetragonal and/or cubic and monoclinic phases. Though this conclusion broadly agrees with the results of the X-ray phase analysis (Table 1) and TEM data [13], some further specificity can be inferred from more detailed data comparison. Thus, broad IR bands and weak Raman spectrum for this sample suggest its strong disordering, first of all, at the level of the nearest coordination sphere and the unit cell characterized by these spectral methods. At the same time, TEM data revealed a rather good crystallinity of nanoparticles of both phases, and an amorphous phase was not detected by XRD as a typical halo in the diffraction patterns. This suggests that disordering of both phases is due to point defects (namely, residual hydroxyls and cation and anion vacancies) still remaining in the lattice of both phases formed after rather soft dehydroxylation. Hence, the nearest coordination sphere of Zr cations in both phases present in this sample appears to be rather distorted, as was earlier proposed for so-called t-ZrO_2 phase by Caracoche et al [27] on the bases of perturbed angular correlation spectroscopy results. Indeed, XAS spectroscopy data [17] revealed for the cubic and monoclinic zirconia phase, a similar Zr–O polyhedron with a sevenfold coordination and a comparable bond length, along with a large distortion or splitting of the next-nearest-neighbor Zr–Zr shell.

For sample calcined at 500 °C, the splitting of IR bands at 355–374, 413–448 and 570–617 cm^{-1} becomes apparently (Fig. 2) driven by the progressive dehydroxylation (Fig. 3) and nearly complete transformation of the cubic phase into the monoclinic one (Table 1). On the whole, by bands position and their relative intensity, this spectrum corresponds to the spectrum of m-ZrO_2 [16]. Again, a rather small difference of this spectrum with the spectrum of the sample calcined at 400 °C, despite nearly complete disappearance of the cubic phase, agrees with the similarity of the Zr–O coordination polyhedra in both phases. On the contrary, the intensity of the Raman bands for this sample is strongly enhanced (Fig. 4), their position mainly corresponding to m-ZrO_2 [16]. Weak bands at 146 and 256 cm^{-1} typical for the t-ZrO_2 are still observed, thus suggesting existence of a small admixture of this phase.

For samples calcined at 600 and 650 °C, the IR spectra differ only slightly from that of samples calcined at 500 °C (Fig. 2), only narrowing of bands is observed, thus suggesting the increase of the lattice ordering due to removal of residual hydroxyls and annealing of point defects. Some redistribution of the intensities of bands at 413 and 448 cm^{-1} is registered.

In contrast, strong variation is observed in the Raman spectra of these samples (Fig. 4). While for the sample annealed at 600 °C the intensity of lines corresponding to the m-zirconia declines, the spectrum completely disappears for the sample calcined at 650 °C. For the sample annealed at 600 °C, weak lines at ~136, ~270 and ~640 cm^{-1} appear which are close by position to those typical for the t-ZrO_2 phase. This agrees with the increase of the content of t-ZrO_2 phase for these samples by XRD (Table 1) and TEM [13] data. Complete disappearance of the Raman spectrum for the sample with a high density of polysynthetic twins is quite surprising and has no analogs in the accessible literature on zirconia. However, similar phenomena were observed when studying the Raman spectra of ceria doped by rare-earth cations [28]. In these systems, the increase of the dopant content leading to progressive ordering of the dopants and oxygen vacancy distribution in the lattice was also accompanied by the disappearance of the Raman spectra while all XRD data were well fitted by the cubic $Fm\bar{3}m$ space group. Hence, some ordering in the defects distribution in the lattice is indeed able to cause disappearance of the Raman spectra.

This suggests that in a similar way ordered defects—polysynthetic twins observed by TEM in zirconia samples calcined at 600–650 °C are able to suppress the Raman spectra.

In agreement with this hypothesis, disappearance of polysynthetic twins in samples calcined at 750 and 1000 °C recovers the Raman spectra, while the IR bands position and splitting remain practically unchanged (Figs. 2 and 4).

3. Modeling of XRD patterns

For dispersed materials, appearance of new peaks is known to be often generated by their disordering [29]. The monoclinic structure of ZrO_2 ($a = 5.315$ Å, $b = 5.208$ Å, $c = 5.148$ Å; $\beta = 99.2$o, S.G. $P2_1/c$) [30] can be considered as comprised of alternating layers of oxygen and zirconium ions situated along the (001) plane. For samples calcined at 600–650 °C, HRTEM data revealed [13] polysynthetic twins, so that crystallites are comprised of the alternating slabs with a mirror symmetric structure. Here, the thickness of slabs, their stacking and alteration can vary.

By using the program for simulation of the diffraction patterns of layered structures [15], diffraction patterns from polysynthetically twinned particles of the monoclinic ZrO_2 with sizes up to 300 Å have been computed.

The starting data for calculation include distribution of atoms in two-dimensionally ordered layers; number of types of different layers (W_N); their stacking order determined by the probability of appearance of a K-type layer after a M-type layer (P_{KM}).

In the two-dimensional ordered layer, the distribution of atoms was determined by parameters of the two-dimensional unit cell (A, B, angle β), the layer thickness C, coordinates x_i, y_i, z_i in the relative units with respect to A, B, C parameters.

In our case, for the direction of the uniaxial disordering, the [001] direction was chosen as a direction of the oxygen layers stacking (Fig. 5). The unit cell parameters of the two-dimensional layer—A, B, and β were equal to parameters a, b, and β of the monoclinic ZrO_2 structure. In different series of modeled diffraction patterns, the layer thickness C was equal to 1, 2 or 3 monoclinic structure units. Coordinates x_i, y_i и z_i were derived by corresponding calculation from the atom coordinates in the monoclinic zirconia unit cell. In each modeling series, two types of layers were used, including one described above (layer 1) and another related by the mirror reflection in the (001) plane (layer 2). The layer thickness was constant, and, as variables, the relative number of layers and their stacking order were used.

Fig. 6 shows model diffraction patterns with different alternation probabilities of layers 1 and 2 at the each layer thickness equal to the c parameter of the monoclinic phase unit cell ($C = c$) and an equal number of both types of layers ($W_1 = W_2 = 0.5$). In the case of the strict alternation order (after layer 1 only layer 2 appears, and vice versa, $P_{11} = 0$), the diffraction pattern contains a peak at position corresponding to the (111) peak of the cubic phase (Fig. 6.1). In this model diffraction pattern, the peaks corresponding to ($\bar{1}11$) and (111) reflections of the monoclinic phase are absent. As P_{11} increases, the diffraction peak broadens (Fig. 6.2 and 6.3), and when only identical layers alternate (the twinned particle contains only one twinning plane), the diffraction pattern corresponds to the monoclinic phase (Fig. 6.5). Hence, at a given layer thickness, it is impossible to obtain the diffraction pattern containing reflections of both cubic and monoclinic phases.

For the triplicate layer thickness ($C = 3c$), keeping number of different layers equal ($W_1 = W_2 = 0.5$), diffraction peaks corresponding by position to both monoclinic and cubic phases are observed (Fig. 7.1). With the increase of P_{11}, the peak corresponding to the cubic phase is smeared, though its integral intensity is preserved until its complete disappearance (Fig. 7.2–4). Only when the relative number of different layers in the particle is changed ($W_1 = 0.3$; $W_2 = 0.7$) while the layer thickness is preserved, the ratio of the integral intensities of "cubic" and "monoclinic" diffraction peaks decreases (Fig. 8). The

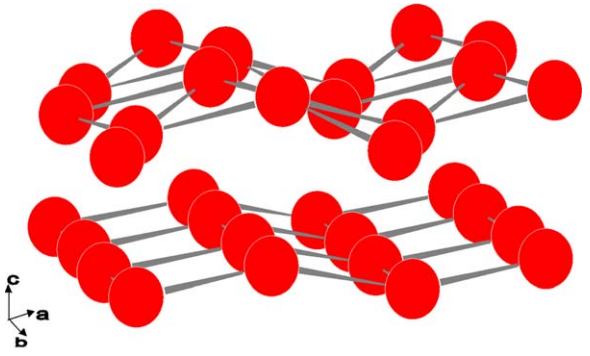

Fig. 5. The layered structure of the oxygen sublattice of monoclinic ZrO_2.

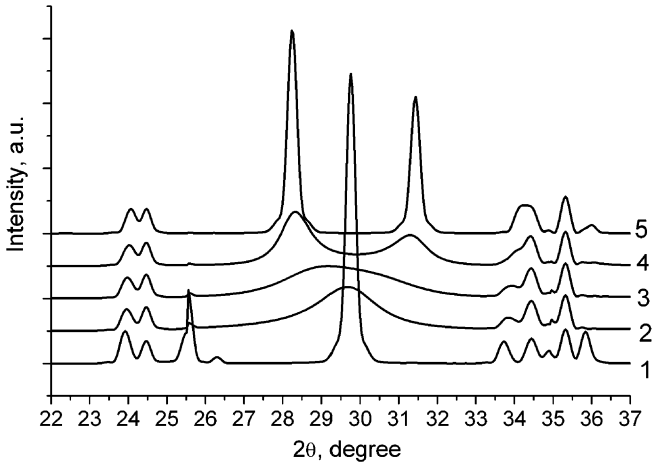

Fig. 6. Simulated diffraction patterns for model particles of zirconium dioxide: $A = a$, $W_1 = 0.5$: 1—$P_{11} = 0$, 2—$P_{11} = 0.5$, 3—$P_{11} = 0.6$, 4—$P_{11} = 0.8$, 5—$P_{11} = 1.0$.

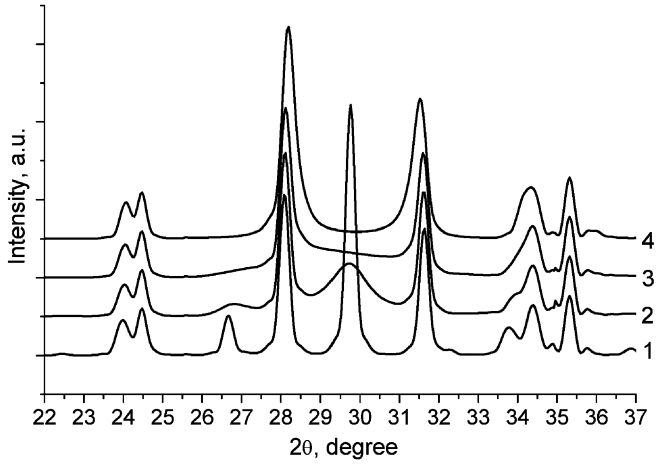

Fig. 7. Simulated diffraction patterns for model particles of zirconium dioxide: $C = 3c$, $W_1 = 0.5$: 1—$P_{11} = 0$, 2—$P_{11} = 0.3$, 3—$P_{11} = 0.5$, 4—$P_{11} = 0.8$.

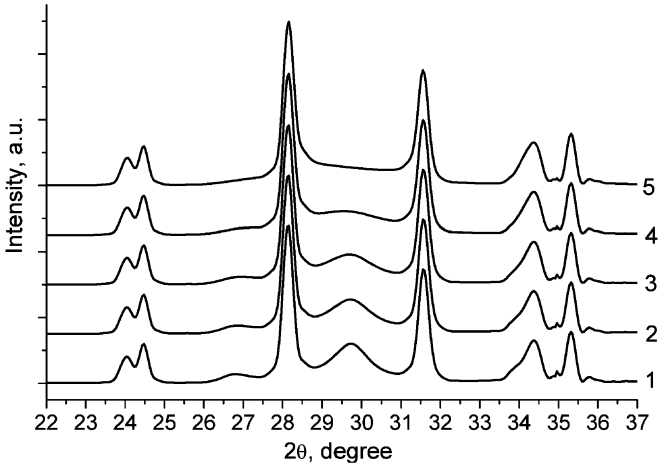

Fig. 8. Simulated diffraction patterns for model particles of zirconium dioxide: $C = 3c$, $W_1 = 0.3$: 1—$P_{11} = 0$, 2—$P_{11} = 0.05$, 3—$P_{11} = 0.1$, 4—$P_{11} = 0.2$, 5—$P_{11} = 0.3$.

increase of P_{11} from 0 to 0.3 also causes broadening and disappearance of the "cubic" diffraction peak.

Diffraction patterns the most close to the experimental one are ensured by models with the next parameters: $A = 3a$, $W_1 = 0.3$, $W_2 = 0.7$, $P_{11} = 0$–0.1. However, even in this case, complete coincidence of the theoretical and experimental diffraction patterns is not achieved (Figs. 8 and 9), since modeling is based on invariable monoclinic unit cell parameters. According to TEM data [13], the monoclinic structure is distorted due to twinning (the monoclinic angle and the unit cell parameters are changed from layer to layer). A due regard for these variations is expected to improve agreement between the simulated and experimental diffraction patterns.

Hence, experimental diffraction patterns for samples calcined at 600 and 650 °C (Fig. 1) formally corresponding to a mixture of the cubic and monoclinic phases can also be

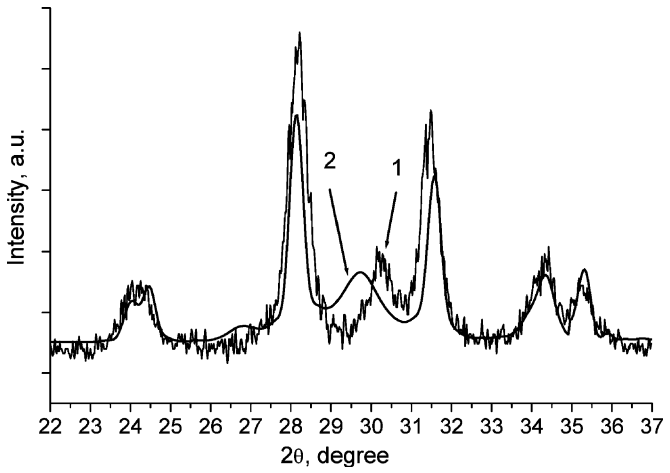

Fig. 9. Fragment of the experimental diffraction pattern of the sample calcined at 600 °C (1) in comparison with the theoretical curve for the model twinned particles (2).

explained as emerging due to multiply twinned particles of the monoclinic phase.

4. Conclusions

A mild HTT of a precipitated hydrous zirconia makes its local structure similar to that in m-ZrO_2, apparently by facilitating polymerization of polynuclear Zr hydroxocomplexes based on a tetramer $[Zr_4(\mu\text{-}OH)_8(OH)_8 \cdot (H_2O)_8] \times H_2O$ via olation and oxolation. This allows to obtain, at low (~400–500 °C) calcination temperatures, nanosized m-ZrO_2 phase with the particle sizes below the critical value determined by the simple end-point thermodynamic analysis of Garvie [31]. The relative stability of these particles to sintering and transformation to c/t-ZrO_2 is ensured by a high content of residual water/hydroxyls in the structure. At higher calcination temperatures, a "pseudocubic" (111) XRD peak reappears, though the amount of the monoclinic phase determined by using the external standard remains nearly constant. Modeling of the XRD diffraction patterns by using approaches earlier developed for layered structures allowed to explain this phenomenon by the polysynthetic mirror twinning along the $(001)_m$ oxygen planes revealed by HRTEM [13]. These periodic planar defects and associated strains affect the mode of ZrO_7 coordination polyhedra ordering in slabs between the adjacent twin planes, which is reflected in the disappearance of the Raman spectra. At higher (>700 °C) calcination temperatures polysynthetic twins as well as associated features in the XRD diffraction patterns disappear while the Raman spectra are restored. Hence, in contrary to single crystals and thin films where those defects are known to be stable, in pure nanozirconia, polysynthetic twins are observed only in the process of the real structure evolution caused by progressive annealing/sintering, which suggests their relative high excess energy caused by their structural specificity.

References

[1] J.B. Goodenough, Nature 404 (2000) 821.
[2] T. Ishikawa, H. Yamaoka, Y. Harada, T. Fujii, T. Nagasawa, Nature 416 (2002) 64.
[3] R.H.J. Hannink, P.M. Kelly, B.C.J. Muddle, J. Am. Ceram. Soc. 83 (2000) 461.
[4] K. Tanabe, Mater. Chem. Phys. 13 (1985) 347.
[5] Y. Nakano, T. Lizuka, H. Hattori, K.J. Tanabe, J. Catal. 57 (1979) 1.
[6] M.M.V.M. Souza, M. Schmal, Appl. Catal. A: General 255 (2003) 83.
[7] A.T. Bell, Stud. Surf. Sci. Catal. 136 (2001) 13.
[8] O.V. Metelkina, V.V. Lunin, V.A. Sadykov, G.M. Alikina, R.V. Bunina, E.A. Paukshtis, V.B. Fenelonov, A.Yu. Derevyankin, V.I. Zaikovskii, U. Schubert, J.R.W. Ross, Catal. Lett. 78 (2002) 111.
[9] G.K. Chuah, S. Jaenicke, B.K.J. Pong, J. Catal. 175 (1998) 80.
[10] E. Tani, M. Yoshimura, Sh.Sōmiya,, J. Am. Ceram. Soc. 66 (1983) 11.
[11] G.K. Chuah, Catal. Today 49 (1999) 131.
[12] S. Benref, E.J. Knözinger, Mater. Chem. 9 (1999) 1203.
[13] V.A. Sadykov, V.I. Zaikovskii, D.A. Zyuzin, E.M. Moroz, E.B. Burgina, A.V. Ishchenko, V.G. Kostrovskii, V.A. Matyshak, Mater. Res. Soc. Symp. Proc. 878E (2005) Y4.8.1-6.
[14] R.C. Garvie, P.S. OLE_LINK1Nicholson, J. Am. Ceram. Soc. 55 (1972) 303.
[15] S.V. Cherepanova, S.V. Tsybulya, J. Mol. Catal. 158 (2000) 263.
[16] P. Bouvier, H.C. Gupta, G.J. Lucazeau, J. Phys. Chem. Solids 62 (2001) 873.
[17] P. Li, I.-W. Chen, J.E. Penner-Hahn, Phys. Rev. B. 48 (1993) 10063.
[18] L.M. Zaitsev, Russ. J. Inorg. Chem. (Engl. Transl.) 11 (1966) 900.
[19] P.N. Kuznetsov, L.I. Kuznetsova, A.M. Zhizhaev, S.M. Kolesnikova, G.L. Pashkov, V.V. Boldyrev, Zh. Neorg. Khim. 47 (2002) 450.
[20] C.M. Phillippi, K.S. Mazdiyasni, J. Am. Ceram. Soc. 54 (1971) 254.
[21] A. Feinberg, C.H. Perry, J. Phys. Chem. Solids 42 (1981) 513.
[22] C.H. Perry, D.-W. Liu, R.P. Ingel, J. Am. Ceram. Soc. 68 (1985) 184.
[23] B.-K. Kim, J.-W. Hahn, K.R. Han, J. Mater. Sci. Lett. 16 (1997) 669.
[24] M. Ishigame, T. Sakurai, J. Am. Ceram. Soc. 60 (1977) 367.
[25] Yu.K. Voron'ko, A.A. Sobol', S.N. Ushakov, L.I. Tsymbal, Neorg. Mater. 3 (1994) 803.
[26] M. Li, Zh. Feng, G. Xiong, P. Ying, Q. Xin, C. Li, J. Phys. Chem. B. 105 (2001) 8107.
[27] M.C. Caracoche, P.C. Rivas, M.M. Cervera, R. Caruso, E. Benavides, O. de Sanctis, S.R. Mintzer, J. Mater. Res. 18 (2003) 208.
[28] V.A. Sadykov, T.G. Kuznetsova, G.M. Alikina, Y.V. Frolova, A.I. Lukashevich, Y.V. Potapova, V.S. Muzykantov, V.A. Rogov, V.V. Kriventsov, D.I. Kochubei, E.M. Moroz, D.A. Zyuzin, V.I. Zaikovskii, V.N. Kolomiichuk, E.A. Paukshtis, E.B. Burgina, V.V. Zyryanov, N.F. Uvarov, S. Neophytides, E. Kemnitz, Catal. Today 93–95 (2004) 45.
[29] V.A. Drits, C. Tchoubar, X-ray Diffraction by Disordered Lamellar Structures, Springer, Berlin, 1990.
[30] B. Bondars, G. Heidemane, J. Grabis, K. Laschke, H. Boysen, J. Schneider, F. Frey, J. Mater. Sci. 30 (1995) 1621.
[31] R.C. Garvie, J. Phys. Chem. 82 (1978) 218.